BIODIVERSITAS
Volume 25, Number 4, April 2024
Pages: 1691-1702

ISSN: 1412-033X
E-ISSN: 2085-4722
DOI: 10.13057/biodiv/d250439

A phenology-based linear spectral unmixing method for rice varieties identification from Landsat 8 Satellite Image in Ngawi District, East Java, Indonesia

IQBAL MAULANA CIPTA[1,2], LALU MUHAMAD JAELANI[1,♥], HARTANTO SANJAYA[1,3]

[1]Department of Geomatics Engineering, Faculty of Civil, Planning and Geo-Engineering, Institut Teknologi Sepuluh Nopember. Jl. Raya ITS, Keputih, Sukolilo, Surabaya 60111, East Java, Indonesia. Tel.: +62-31-5929486, ♥email: lmjaelani@its.ac.id
[2]Monash University Indonesia. Green Office Park 9, The Breeze BSD City, South Tangerang 15345, Banten, Indonesia
[3]National Research and Innovation Agency. Jl. M.H. Thamrin No. 8, Central Jakarta 10340, Jakarta, Indonesia

Manuscript received: 7 February 2024. Revision accepted: 22 April 2024.

Abstract. *Cipta IM, Jaelani LM, Sanjaya H. 2024. A phenology-based linear spectral unmixing method for rice varieties identification from Landsat 8 Satellite Image in Ngawi District, East Java, Indonesia. Biodiversitas 25: 1691-1702.* Ngawi District is a prominent rice-producing district in East Java, Indonesia. Based on the BPS data from 2021, Ngawi District yielded a total of 786.49 thousand tons of paddy. Multiple strategies to enhance rice production include enhancing rice productivity, increasing paddy fields, and using effective land management techniques. Utilizing a superior breed of seeds can augment productivity. Remote sensing can be utilized to obtain such data, one of which is the Linear Spectral Unmixing (LSU) technique. The LSU approach is used to determine the proportion of a pure object's presence in a pixel. The Inpari 32 rice variety is the predominant type identified from the analysis of the processing outcomes utilizing satellite imagery. In addition, validation was performed by utilizing many sample locations distributed around Ploso Lor and Rejuno Villages, resulting in consistent findings between the data analysis and the actual conditions observed in the field. The RMSE calculation was conducted on both sets of processing results, and the most optimal RMSE value was achieved when processing was performed using Landsat 8 image data, yielding an RMSE value of roughly ±1.2%. The accuracy of the model was evaluated using a confusion matrix, which yielded an overall accuracy rate of 86.67%.

Keywords: Inpari 32, remote sensing, rice plants, RMSE, sustainability, Worldview 2

INTRODUCTION

Rice (*Oryza sativa* L.) is the primary food crop for a significant portion of the global population, with over half of the world's seven billion people relying on it. The majority of rice consumption, exceeding 90%, takes place in Asia (Bandumula 2018; Dineshkumar et al. 2019). According to the United States Department of Agriculture (USDA) data for the 2015/2016 period, the top eight nations in rice production and consumption collectively contribute to around 82.05% of global rice production and 78.23% of its consumption (USDA 2015). Indonesia, ranking third after China and India, produced a total of 35,300,000,000 kg (Maraseni et al. 2018). Rice constitutes the primary dietary staple for a majority of the Indonesian populace. Between 2010 and 2016, both rice production and consumption in Indonesia exhibited growth with average annual rates of 2.34% and 2.32%, respectively (Wahyudi et al. 2019).

According to the Central Bureau of Statistics (BPS), East Java Province, Indonesia emerged as the leading rice producer in Indonesia in 2021, producing 9.90 million tons of milled dry paddy, surpassing all other provinces (BPS 2022). Ngawi District stands as one of the significant rice-producing regencies in East Java. BPS data indicates that Ngawi District recorded a rice production of 786.49 thousand tons in 2021, ranking it second in rice production among regencies, following Lamongan District.

Several strategies can bolster rice production, including enhancing rice productivity, expanding the paddy field acreage, and effectively managing land resources (Singh et al. 2017; Xin et al. 2020; Abdul-Rahaman et al. 2021). Productivity enhancements can be achieved by leveraging high-quality seeds (Hussain et al. 2014; Ghimire et al. 2015; Sarangi et al. 2016). The distribution of superior seed varieties can be identified using remote sensing techniques, specifically spectral classification employing the Linear Spectral Unmixing (LSU) method (Xu et al. 2017; Yu et al. 2017). The LSU method is a prevalent technique for extracting information from mixed pixels, identifying the proportion of pure object (endmember) presence within a pixel. To apply the linear spectral unmixing method, endmembers for each object must be determined (Keshava and Mustard 2002; Keshava 2003; Bai et al. 2012; Tompolidi et al. 2020; Cipta et al. 2022).

While initially employed for the interpretation of hyperspectral images, such as High Spectral Resolution Advanced Visible/Infrared Image Spectrometer (HSR AVIRIS), the LSU classification has evolved to analyze multispectral imagery. This method's versatility has been illustrated in the work of Bai et al. (2012), where Landsat 7 ETM+ data was utilized to estimate forest coverage in Pingnan County. Similarly, Tompolidi et al. (2020)

employed spectral unmixing methods to map hydrothermal land with multispectral data from ASTER, Landsat 8, and Sentinel 2.

Remote sensing methods can also be utilized to monitor plant phenology, studying how organisms like plants and animals respond to changes in climate shifts (Liang 2019). Phenology monitoring has been extensively studied. Zhang et al. (2003) monitored vegetation phenology using MODIS satellite imagery and the Enhanced Vegetation Index (EVI). Dineshkumar et al. (2019) observed the phenology of rice crops using MODIS satellite data and the EVI spectral index. Additionally, Zhao et al. (2021) monitored rice crop phenology using Sentinel 2 and MODIS satellite imagery, incorporating the NDVI and Land Surface Water Index (LSWI) spectral indices.

In the present study, rice plant phenology was assessed using MODIS satellite imagery data and spectral indices such as NDVI, EVI, LSWI, and MNDWI. Subsequently, the phenology data and in-situ endmembers were used to identify rice varieties from Landsat 8 Imagery using the LSU method. The study aims to furnish valuable insights into the rice plant calendar and to present spatial data through a map illustrating the distribution of various rice varieties.

MATERIALS AND METHODS

Study area

The study was carried out in the villages of Ploso Lor and Rejuno, located in Ngawi District, East Java, Indonesia (Figure 1). The villages of Ploso Lor and Rejuno have geographic coordinates spanning from 111°36'16.9" E to 111°38'56.5" E and 7°25'50.3" S to 7°27'2.3" S. Ploso Lor village covers an area of 3.92 km^2, while Rejuno village spans across 12.81 km^2. Located on the northeastern side of Ngawi District, both villages share a border with Bojonegoro District.

Materials

This study utilized the Landsat 8 images sourced as surface reflectance data from the Google Earth Engine platform. The acquisition time was tailored to align with the reproductive phase of rice plants in the Ngawi District. The Landsat 8 satellite imagery was processed using the Linear Spectral Unmixing (LSU) algorithm. Additionally, the study utilized MODIS MCD43C4- MODIS/Terra + Aqua Nadir BRDF satellite images acquired through the Google Earth Engine platform between January 2011 and December 2022. Sentinel 1 GRD satellite images, sourced from the same platform, were used with an acquisition timeframe spanning January 2015 to December 2022. These MODIS and Sentinel 1 GRD satellite data were used to determine rice plant phenology.

Furthermore, this research incorporated Worldview 2 satellite image data obtained from maxar.com on May 25, 2023, for comparative analysis of the data processing outcomes. Vector data representing raw paddy fields in the Ngawi District were obtained from the Ina-Geoportal of the National Geospatial Information Agency (BIG, https://tanahair.indonesia.go.id/portal-web) to define the study area boundaries. Lastly, endmember spectral data for each rice variety, acquired through direct field measurements, were utilized to construct spectral libraries for each rice variety.

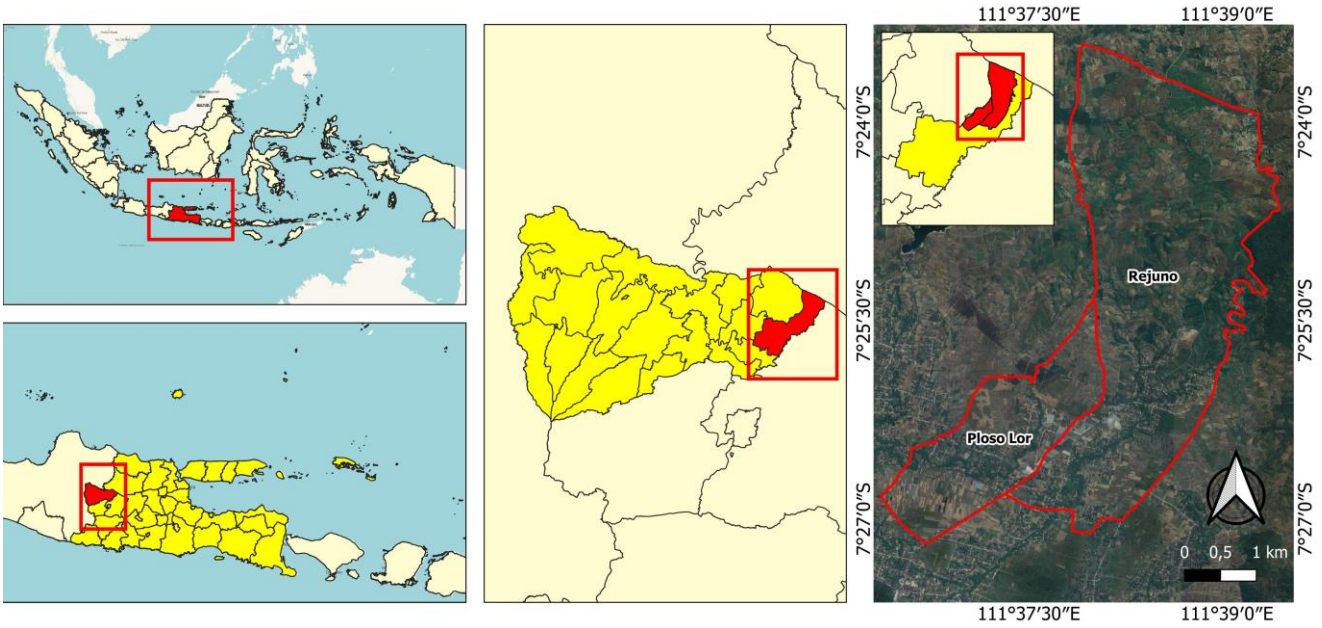

Figure 1. Research area on Rejuno and Ploso Lor Villages, Ngawi District, East Java, Indonesia

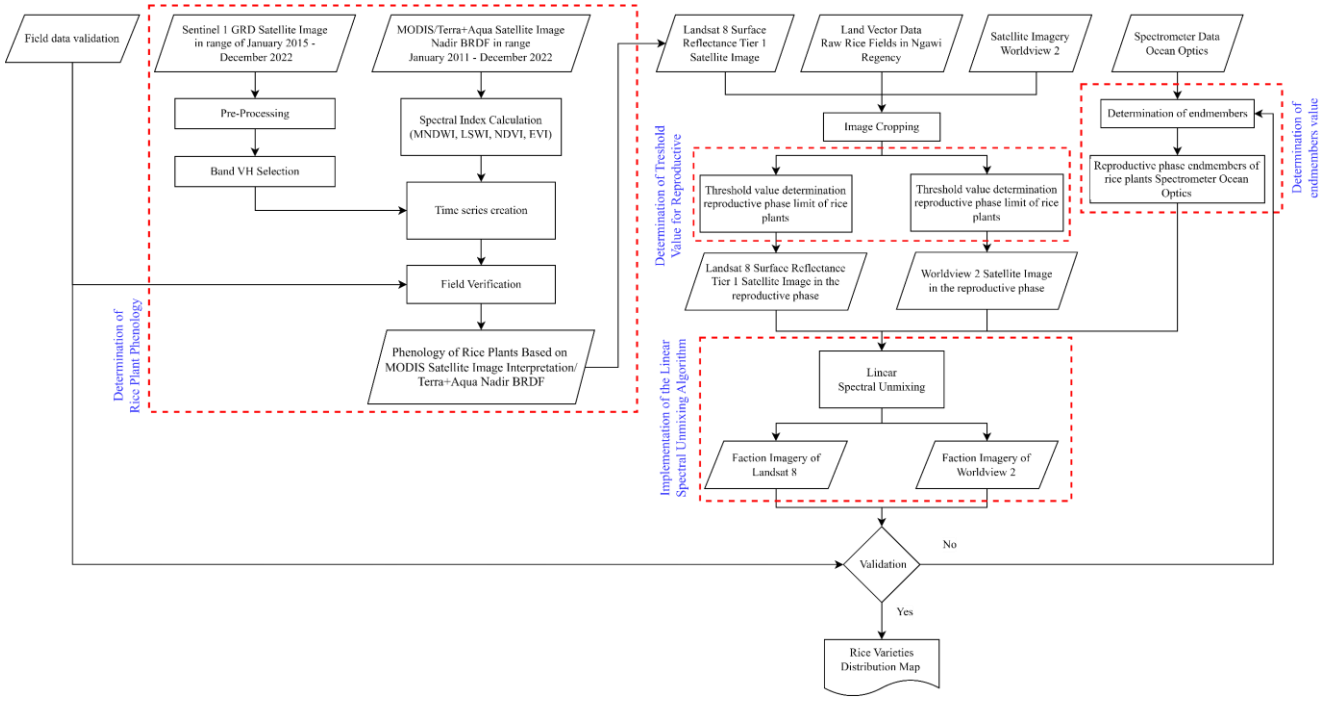

Figure 2. Workflow of the proposed methodology for cropland identification

Methods

Our study was structured into three distinct sections, as illustrated in Figure 2. Initially, spectral indices were calculated using MODIS satellite images and rice plant phenology was determined. Subsequently, we established threshold values to delineate reproductive land areas. Thirdly, endmember values essential for the linear spectral unmixing algorithm were identified. Lastly, the calculation of the linear spectral unmixing algorithm was executed.

Calculation of spectral indices using MODIS Satellite Images and determination of rice plant phenology

Utilizing remote sensing technology, the vegetation phenology cycle was delineated by four key transition dates: (i) Greening, marking the onset of photosynthetic activity; (ii) Maturation, indicating the peak of vegetation greenness; (iii) Senescence, representing the decline in plant photosynthetic activity; and (iv) Dormancy, signifying a period of no physiological activity (Zhang et al. 2003). Rice plants have unique morphological characteristics, continuously growing in flooded soils. The temporal dynamics of the rice plant growth can be classified into three primary stages: (i) Flooding and planting period; (ii) Growth period represented by tillering, flowering, and ripening stages; and (iii) post-harvest fallow period. These characteristics are detectable using remote sensing technology through various spectral indices derived using MODIS/Terra + Aqua Nadir BRDF image data. The utilized MODIS image data spans from January 2011 to December 2022. The spectral indices utilized comprise the Modified Normalized Difference Water Index (MNDWI), Land Surface Water Index (LSWI), Enhanced Vegetation Index (EVI), and Normalized Difference Vegetation Index (NDVI) (Gao et al. 2000; Huete et al. 2002; Potter et al. 2007; Chandrasekar et al. 2010; Bhandari et al. 2012; Szabó et al. 2016; Zhao et al. 2021).

$$\text{MNDWI} = \frac{(\rho GREEN - \rho SWIR)}{(\rho GREEN + \rho SWIR)} \quad (1)$$

$$\text{EVI} = 2.5\ x\ \frac{(\rho NIR - \rho RED)}{(\rho NIR + 6\ x\ \rho RED - 7.5\ x\ \rho BLUE + 1)} \quad (2)$$

$$\text{NDVI} = \frac{(\rho NIR - \rho RED)}{(\rho NIR + \rho RED)} \quad (3)$$

$$\text{LSWI} = \frac{(\rho NIR - \rho SWIR)}{(\rho NIR + \rho SWIR)} \quad (4)$$

Where:

ρ : Surface Reflectance of band-n.

Determination of threshold values for reproductive land separation

Before applying the Linear Spectral Unmixing (LSU) algorithm, it is essential to distinguish between reproductive and non-reproductive land. In this study, the Otsu method was employed to determine threshold values. This method uses histogram analysis to partition the image into distinct segments. Otsu's approach frames image segmentation as an optimization challenge to identify the threshold that optimally distinguishes between the object and its background (Otsu 1979; Pal and Pal 1993; Li and Tam 1998).

$$\sigma^2 = P_{nw} \times (M_{nw} - M)^2 + P_w \times (M_w - M)^2 \quad (5)$$

$$M = P_{nw} \times M_{nw} + P_w \times M_w \quad (6)$$

$$P_{nw} + P_w = 1 \quad (7)$$

$$T = ArgMax\{P_{nw} \times (M_{nw} - M)^2 + P_w \times (M_w - M)^2\} \quad (8)$$

Where:

σ^2 : Within-class variance
P_{nw} : Pixel value probabilities (background)
P_w : Pixel value probabilities (foreground)
M_{nw} : Mean pixel values (background)
M_w : Mean pixel values (foreground)
M : Mean pixel values of the image
T : Threshold value

Determination of endmember values for spectral unmixing algorithm

A spectral library serves as a critical input for the LSU method. In this study, the spectral library was created using an Ocean Optics spectrometer calibrated with white and black references. Sampling for constructing the spectral library was based on the rice plant varieties present in the study area, namely Inpari 32, Cibogo, and MR, focusing on the rice plant endmembers in the generative phase.

Given that Landsat-8 and Worldview-2 satellite images operate on different wavelength ranges compared to the spectrometer, adjustments were required to align the wavelength ranges of these satellite images with the spectrometer's (refer to Tables 1 and 2). The Landsat-8 satellite bands utilized in this study comprised band-1 (coastal aerosol), band-2 (Blue), band-3 (Green), band-4 (Red), and band-5 (NIR). The Worldview-2 satellite bands included band-1 (Blue), band-2 (Green), band-3 (Red), and band-4 (NIR).

Calculation of LSU algorithm

LSU is a technique where the spectral values of pixels containing a mixture of materials are separated into individual spectral components called endmembers. Additionally, fraction maps or grayscale maps are generated to represent the proportions of each endmember within the pixel (Keshava 2003; Keshava and Mustard 2002; Singer and McCord 1979). The mathematical formula for linear spectral unmixing is expressed as follows.

$$R_i = \sum_{k=1}^{n} f_k R_{ik} + ER_i \quad (9)$$

Where:
i : 1, …, m (number of spectral bands)
k : 1, …, n (number of endmembers)
R_i : Value of a pixel in bands i
f_k : Fraction of endmember k in that pixel
R_{ik} : Reflectance of endmember k in bands i
ER_i : Unmodeled residual in bands i

Table 1. Endmember value of rice variety on Landsat 8

Bands	Reflectance Value (ρ)		
	Inpari 32	Cibogo	MR
Band-1 (Coastal aerosol)	0.0296	0.0016	0.2104
Band-2 (Blue)	0.0375	0.0181	0.1303
Band-3 (Green)	0.1303	0.1088	0.1518
Band-4 (Red)	0.0483	0.0097	0.0784
Band-5 (NIR)	0.5428	0.2116	0.6615

Table 2. Endmember value of rice variety on Worldview 2

Bands	Reflectance Value (ρ)		
	Inpari 32	Cibogo	MR
Band-1 (Blue)	0.0255	0.0082	0.0151
Band-2 (Green)	0.1342	0.1336	0.0941
Band-3 (Red)	0.0332	0.0047	0.0413
Band-4 (NIR)	0.4790	0.3564	0.3162

The model residual error assesses the LSU model (ER_i), reported as the root mean squared error (RMSE) from formula 10 (Weng et al. 2004; Kärdi 2007; Daldegan et al. 2019).

$$RMSE = \sqrt{\frac{\sum_{i=1}^{m}(ER_i)^2}{m}} \quad (10)$$

RESULTS AND DISCUSSION

Phenology of rice plants

The monitoring of rice plant phenology in this study relies on spectral index values from MODIS image data and SAR Sentinel 1 data spanning from 2012 to 2022. Figure 3 represents the response of rice fields to spectral index values over a decade. Analysis of the 10-year phenological data reveals recurring patterns in spectral indices and backscatter characteristics annually. These patterns suggest that rice plants undergo three distinct phases each year.

Figure 4 represents the initial planting season in 2022. A rise in NDVI, LSWI, and EVI values signifies the vegetative phase. The elevated MNDWI value at the onset of the vegetative phase corresponds to the presence of water in the rice field. As the rice plants mature and their foliage thickens, the satellite sensor captures reduced information about the soil and water, leading to diminished MNDWI values. The backscatter value increased at the start of the vegetative phase, stabilizing towards its end and persisting into the subsequent phase.

The reproductive phase was characterized by a decline in NDVI, LSWI, and EVI values from their peak levels during this stage. Meanwhile, the MNDWI value maintained a consistent level throughout the reproductive phase. The backscatter value increased during this phase, having remained relatively stable in the preceding phase.

The ripening phase was characterized by the NDVI, LSWI, EVI, and MNDWI values approaching their minimum. Similar to the previous phase, the MNDWI value remained relatively stable. Conversely, the backscatter value diminished during the ripening phase following an increase in the preceding phase. Utilizing the 10-year phenology data, planting patterns and calendars were established, as depicted in Figure 5.

Figure 5 shows that the rice cultivation season occurred three times in a year, depicted by blue-colored boxes. The vegetative phase of rice plants took place in the months: (i) early December - mid-January; (ii) early April - mid-May; (iii) early August - mid-September. The vegetative phase in Figure 5 is represented by green-colored boxes. The reproductive phase of rice plants occurred in the months: (i) late January - mid-February; (ii) late May - mid-June; (iii) late September - mid-October. The reproductive phase in Figure 5 is depicted by yellow-colored boxes. The ripening phase of rice plants occurred in the months: (i) mid-February - mid-March; (ii) mid-June - mid-July; (iii) mid-October - mid-November. The ripening phase in Figure 5 is represented by orange-colored boxes.

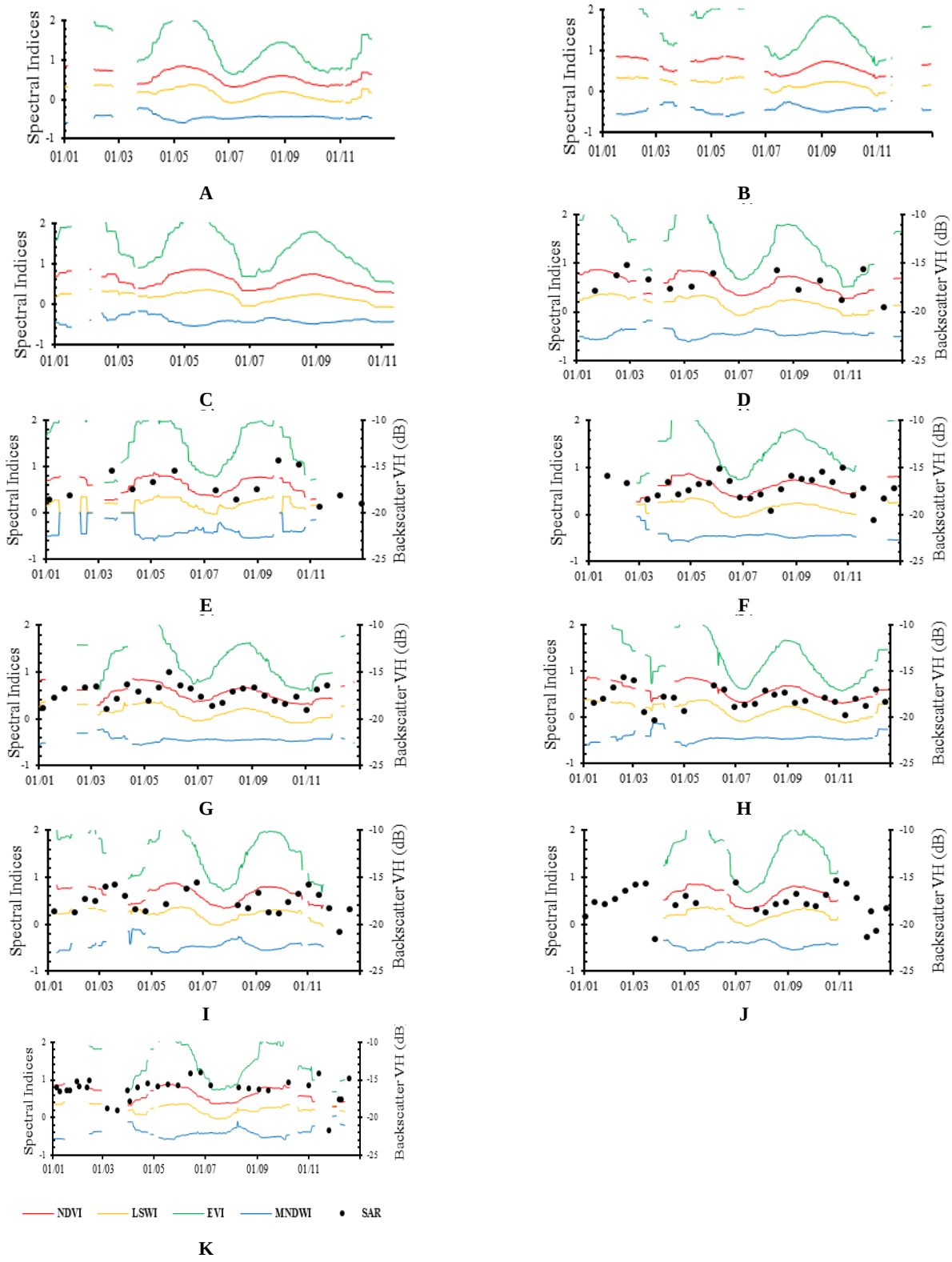

Figure 3. Phenology of paddy rice in 10 years. A. 2012, B. 2013, C. 2014, D. 2015, E. 2016, F. 2017, G. 2018, H. 2019, I. 2020, J. 2021, K. 2022

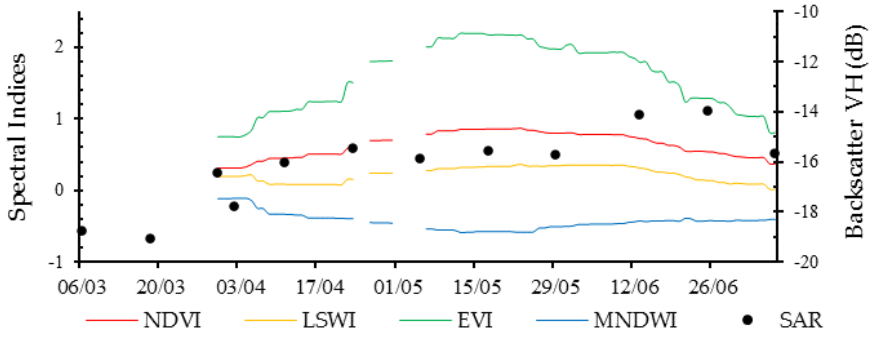

Figure 4. Phenology of paddy rice season 1 in 2022

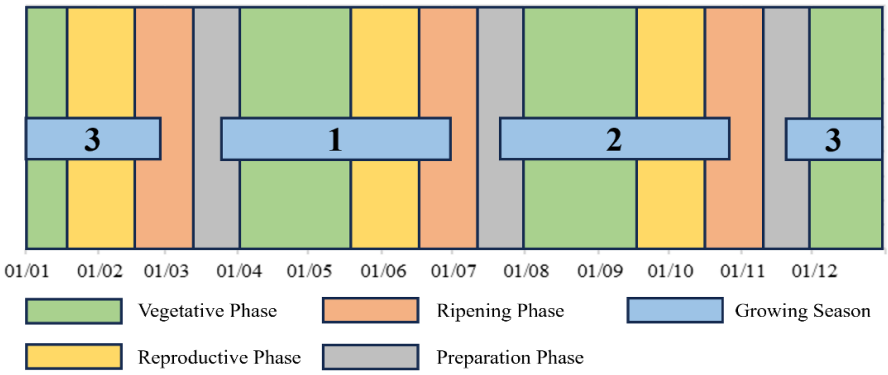

Figure 5. Paddy rice planting calendar

Satellite imagery reproductive phase of paddy

The selection of satellite images used to determine the threshold values was centered on the reproductive phase, as determined by the planting pattern and calendar data shown in Figure 5. This phase was selected due to the dense foliage of rice plants, enhancing their visibility to satellites. The Landsat-8 satellite images used to determine the threshold values were captured on the dates: September 24, 2020; May 22, 2021; June 2, 2022; September 22, 2022; and May 28, 2023.

Table 3 presents the threshold values of spectral indices (NDVI, LSWI, EVI, and MNDWI) for each satellite image during the reproductive phase of rice crops. These threshold values served to distinguish between rice crop areas in reproductive and non-reproductive phases. The average of five threshold values for a specific date was subsequently calculated. The average threshold values for the spectral indices NDVI, LSWI, EVI, and MNDWI were 0.72, 0.31, 0.47, and -0.44, respectively. These threshold values were then employed in both satellite images for the linear spectral unmixing process.

The Landsat-8 image used was acquired on May 28, 2023. This Landsat-8 image was processed by segmenting it according to the administrative boundaries of the Ploso Lor and Rejuno villages. Additionally, the image was subdivided using vector data of paddy field areas (Figure 6. A). After the image segmentation process, the determined threshold values were applied to the reproductive phase, as illustrated in Figure 6.B. The images captured during the reproductive phase served to identify rice plant varieties using the linear spectral unmixing method.

For comparative analysis, the Worldview-2 image was incorporated into this study to evaluate the processed Landsat-8 data. The Worldview-2 image, acquired on May 25, 2023, covered the Ploso Lor and Rejuno villages within Ngawi District. Similar to the Landsat-8 image, this Worldview-2 image was also processed by segmenting it according to the vector data of the paddy field areas (Figure 7. A). After the image segmentation process, the determined threshold values were applied to the reproductive phase. The resulting image showcased a Worldview-2 satellite image captured during the reproductive phase (Figure 7. B).

Table 3. Threshold value of reproductive phase

Dates	Threshold Values Reproductive Phase			
	NDVI	LSWI	EVI	MNDWI
2020/09/24	0.7169	0.2989	0.4902	-0.4707
2021/05/22	0.7425	0.3575	0.4395	-0.3207
2022/06/02	0.7166	0.3183	0.4472	-0.4689
2022/09/22	0.7109	0.2987	0.5136	-0.4746
2023/05/28	0.7247	0.2871	0.4745	-0.4942

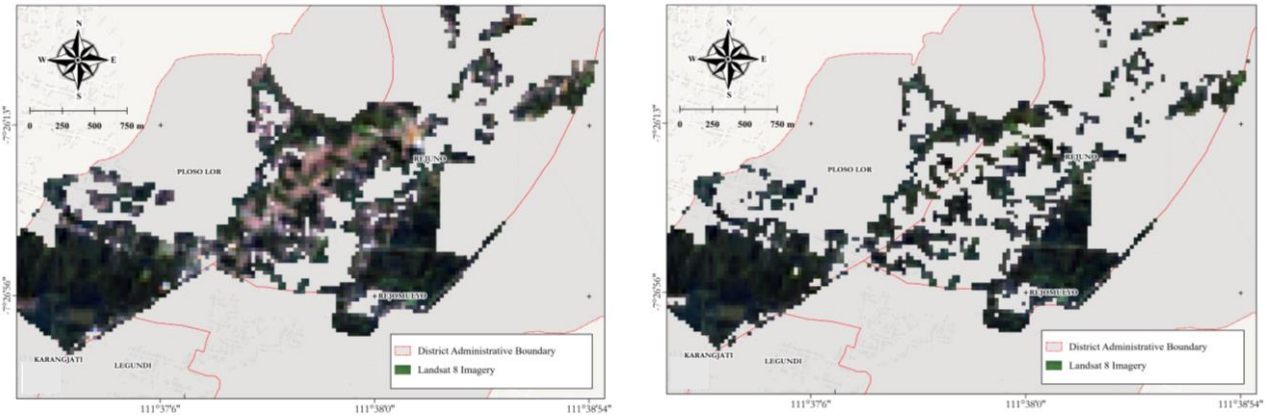

Figure 6. A. Landsat 8 Imagery of paddy fields areas; B. Landsat 8 Imagery of the reproductive phase

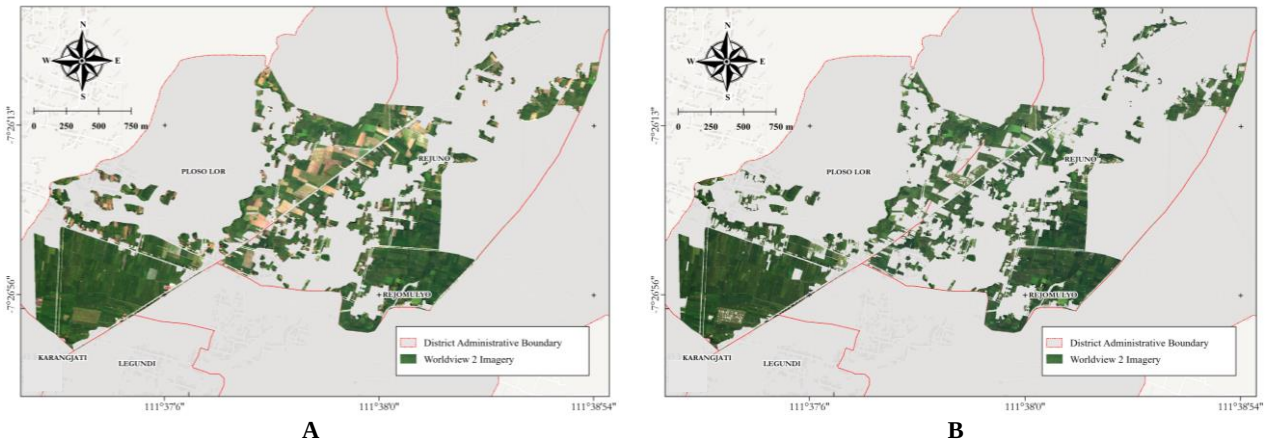

Figure 7. A. Worldview 2 Imagery of Paddy Fields Areas; B. Worldview 2 Imagery of Reproductive Phase

Distribution of rice plant varieties in Ploso Lor and Rejuno Villages

The result of the LSU algorithm is a fraction map for each variety, displaying values ranging from 0 to 1. The fraction maps for Inpari 32, Cibogo, and MR are illustrated in Figure 8.

According to the statistical calculations presented in Table 4, the results of linear spectral unmixing using Landsat 8 image data revealed that the MR and Cibogo varieties registered a value of 0 for each pixel. This suggests the absence of MR and Cibogo varieties in the first planting season of 2023. Conversely, as presented in Table 4 and Figure 9, the Inpari 32 variety exhibited values ranging from 0.41 to 0.89. Within this range, the presence of the Inpari 32 variety is discernible in both villages. Nonetheless, there were values below 0.50, indicating the existence of other varieties within those pixels. Hence, it becomes necessary to distinguish the dominant variety from the rest.

In this study, a threshold value was established to distinguish the dominant variety from other varieties (excluding Inpari 32, Cibogo, and MR). The threshold value used to identify the dominant variety in the fraction maps was set at >0.50. This threshold considered fractions greater than half of the pixel value as indicative of the dominant variety (Figure 10). Based on the data processing results using Landsat 8 satellite images, it was determined that the dominant variety planted by farmers in Ploso Lor and Rejuno villages during the first planting season of 2023 was the Inpari 32 variety.

Table 4. Landsat 8 endmember fraction values range

Varieties	Fractions Percentage Value Range	
	Min	Max
Inpari 32	0.41	0.89
Cibogo	0.00	0.00
MR	0.00	0.00

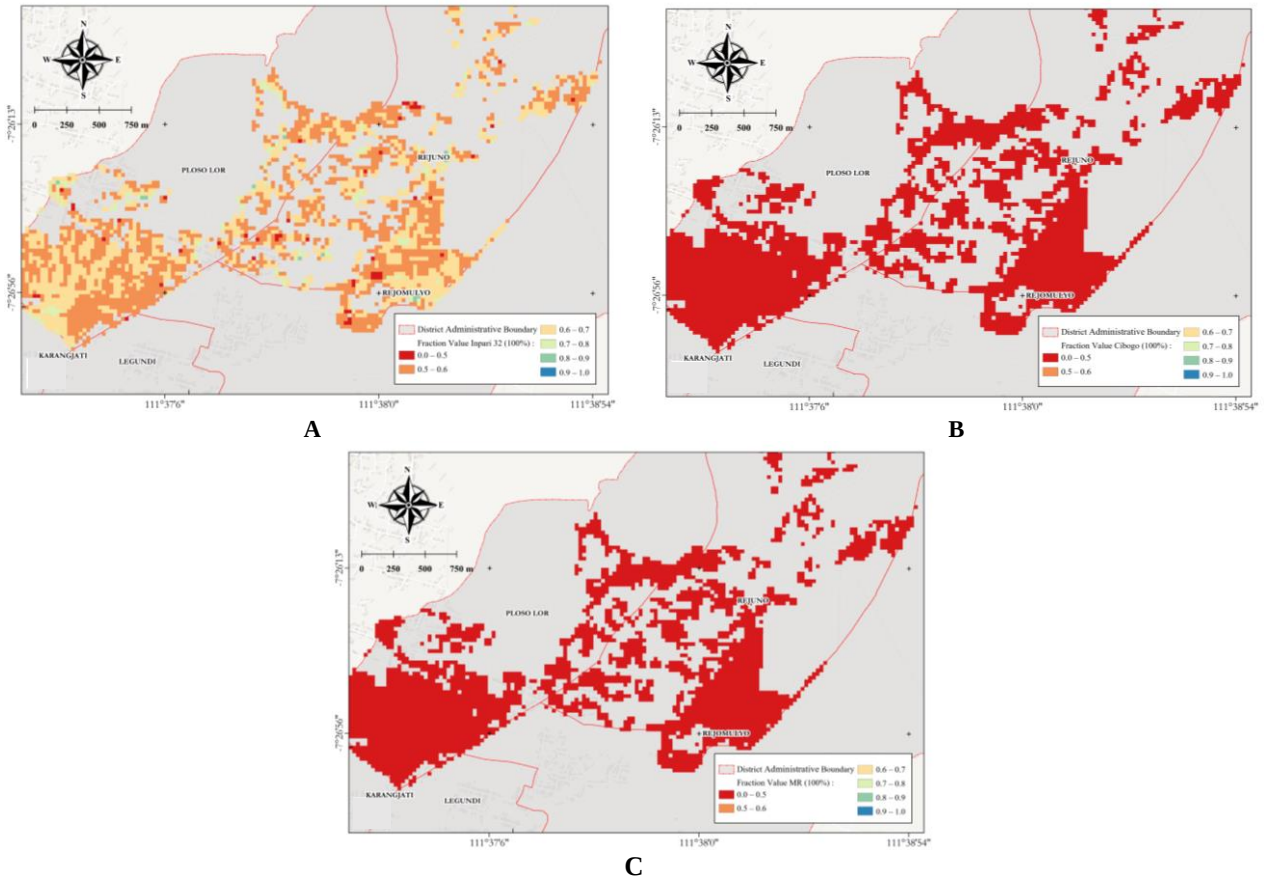

Figure 8. Map fraction result on Landsat 8. A. Inpari 32; B. Cibogo; C. MR

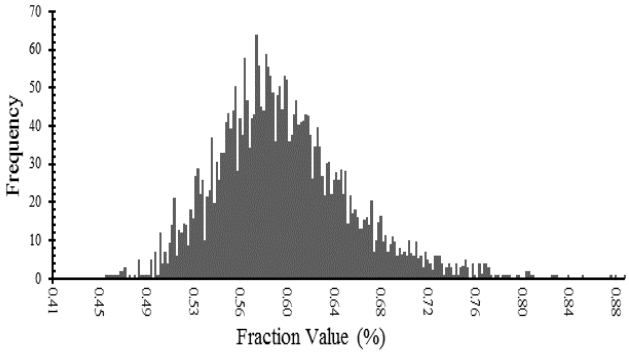

Figure 9. Landsat 8 Inpari 32 fraction map histogram

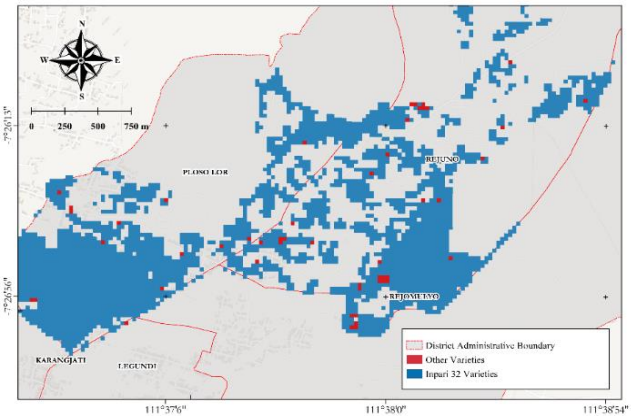

Figure 10. Landsat 8 dominant variety distribution map

A comparison between the LSU results from Landsat-8 data and Worldview-2 data for Ploso Lor and Rejuno Villages, Ngawi District, is presented in Figure 11.

Based on the statistical calculations of the LSU results from Worldview-2 data (Table 5), the Cibogo and MR varieties displayed a value of 0 for each pixel. This indicates that neither the Cibogo nor MR varieties were used in the first planting season of 2023. Conversely, in Figure 12, the Inpari 32 variety exhibited a range of values from 0.41 to 1.26. Within this range, the presence of the Inpari 32 variety was identifiable in both villages. However, with values below 0.5 still present, indicating the potential presence of other varieties in those pixels, it became imperative to differentiate the dominant variety from the others. This was achieved by employing a threshold value above 0.5 for the dominant variety and below 0.5 for the others (Figure 13). Based on the data processing results using the Worldview-2 satellite images, it can be concluded that the dominant variety planted by farmers in Ploso Lor and Rejuno villages during the first planting season of 2023 was the Inpari 32 variety.

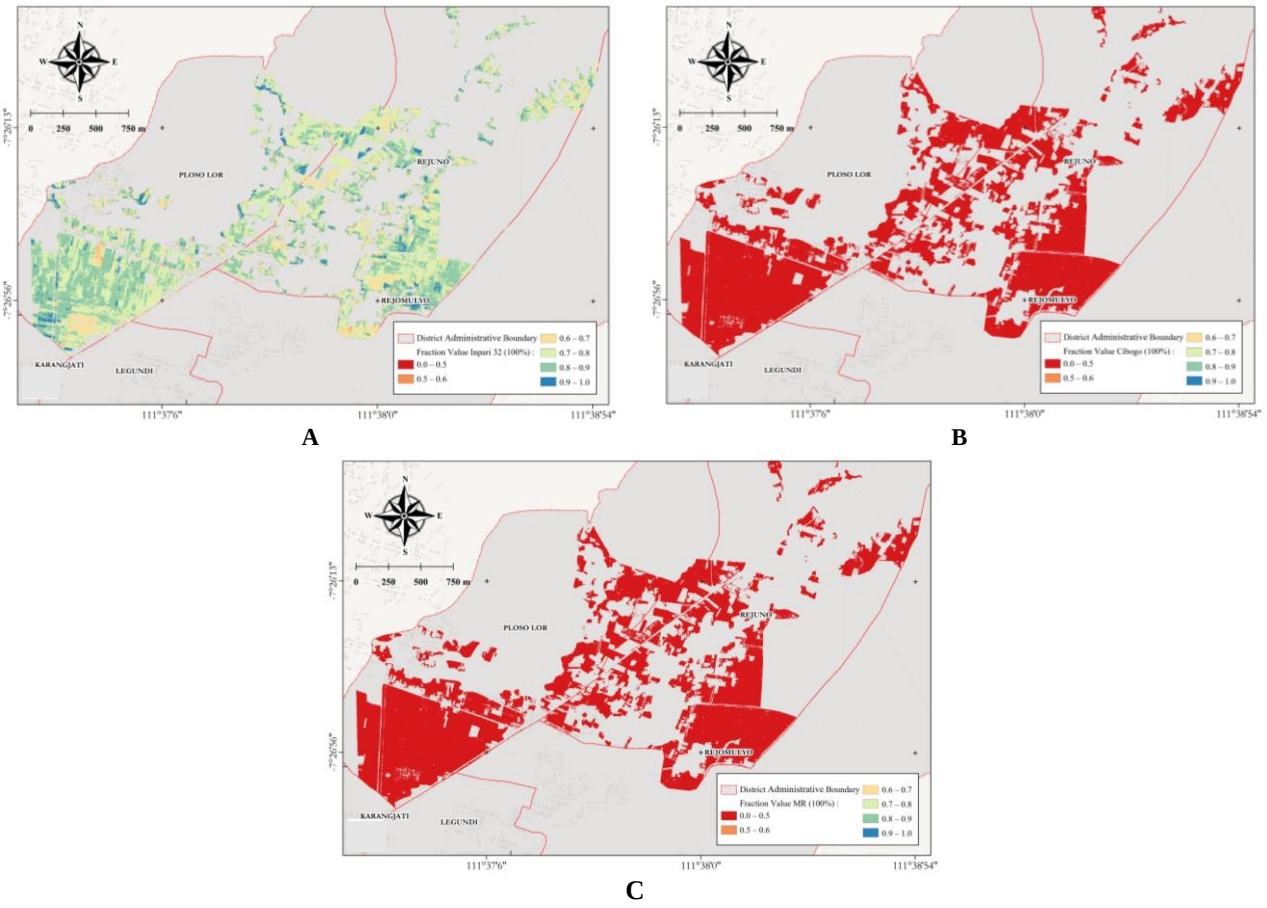

Figure 11. Map Fraction Result on Worldview 2. A. Inpari 32; B. Cibogo; C. MR

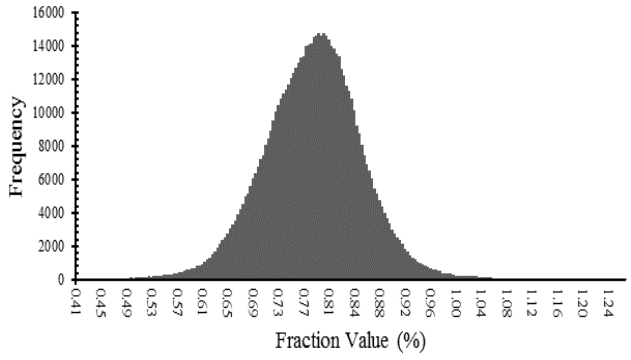

Figure 12. Worldview 2 Landsat 8 Inpari 32 fraction map histogram

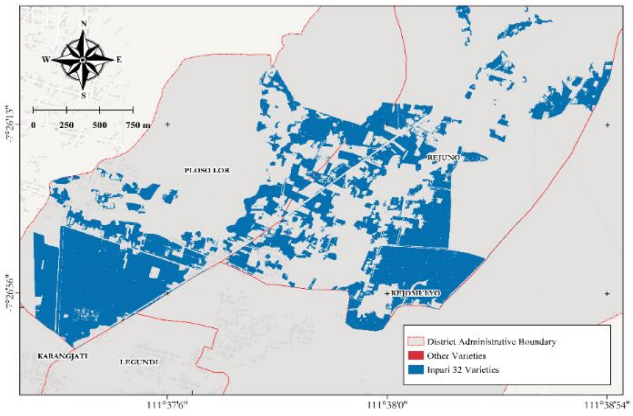

Figure 13. Worldview 2 dominant variety distribution map

Table 5. Worldview 2 endmember fraction value range

Varieties	Fractions percentage value range	
	Min	Max
Inpari 32	0.41	0.89
Cibogo	0.00	0.00
MR	0.00	0.00

Table 6. RMSE value range of both satellite images

Data	RMSE value range			
	Min	Max	Mean	StdDev.
Landsat 8	0.007	0.022	0.012	0.002
Worldview 2	0.055	0.124	0.070	0.004

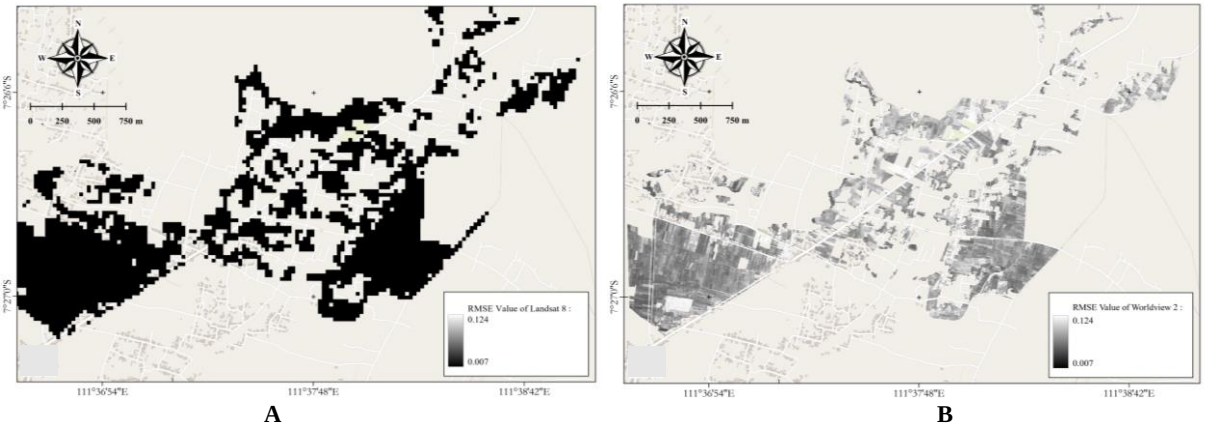

Figure 14. RMSE Fraction Endmember Distribution Map. A. Landsat 8; B. Worldview 2

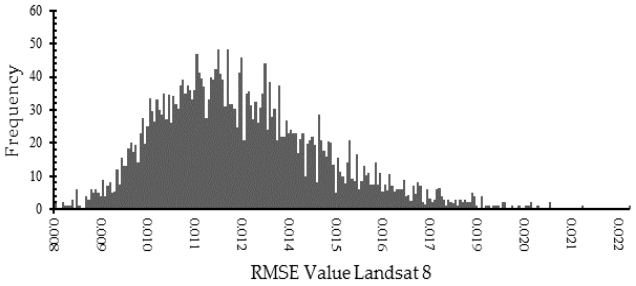

Figure 15. RMSE Value of Landsat 8

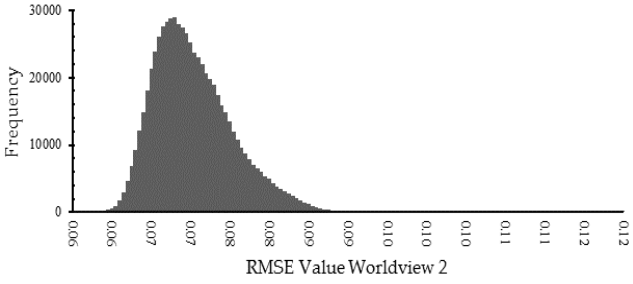

Figure 16. RMSE Value of Worldview 2

RMSE and validation

The model residual error, represented as the Root Mean Squared Error (RMSE), was calculated to evaluate the accuracy of linear spectral unmixing results. The RMSE provided insights into how effectively each endmember pixel was represented in a pixel. The RMSE results for both Landsat 8 and Worldview 2 are depicted in Figure 14.

The RMSE values for Landsat 8 ranged from 0.007 to 0.022 (Table 6), with average and standard deviation RMSE values of 0.012 and 0.002, respectively (Figure 15). In contrast, the RMSE values for Worldview 2 ranged from 0.055 to 0.124, with average and standard deviation RMSE values of 0.070 and 0.004, respectively (Figure 16). These findings suggest that Landsat 8 images yielded better linear spectral unmixing performance, exhibiting smaller RMSE values compared to Worldview 2. The RMSE values translated to an error of approximately ±1.2% in the linear spectral unmixing results of each pixel.

The bandwidth range associated with each satellite image band can influence the RMSE results. Table 7 presents the bandwidth range for specific channels of both Landsat 8 satellite images, sourced from the Google Earth Engine platform (https://developers.google.com) and Worldview 2 satellite images, sourced from the official ESA Space website (https://earth.esa.int).

Based on Table 7, the bandwidth range for each channel on the Landsat 8 satellite was narrower compared to the Worldview 2 satellite. This difference had an impact on the resulting error because the average calculation for determining the endmembers for each rice variety in this study was conducted within the bandwidth range of each channel used. A broader bandwidth range in a satellite image band may not fully capture the values within that range.

Table 7. The bandwidth range on each satellite

Band	Landsat 8 (nm)	Worldview 2(nm)
Coastal Aerosol	16	-
Blue	60	60
Green	57	70
Red	37	60
NIR	28	125

Table 8. Confusion matrix calculation results

Class	Inpari 32	Other	Total	User's accuracy
Inpari 32	12	0	12	100%
Other	2	1	3	33.33%
Total	14	1	15	
Producer's accuracy	85.71%	100%		86.67%

Furthermore, a confusion matrix was calculated to assess the agreement between the linear spectral unmixing processing and the field validation data. Field validation data consists of 15 coordinate points in paddy fields, accompanied by information on the rice plant varieties employed. The results of the confusion matrix are presented in Table 8. Based on Table 8, the accuracy test results using the confusion matrix show a user's accuracy of 100% for the Inpari 32 variety and 33.33% for other varieties. The producer's accuracy was 85.71% for the Inpari 32 variety and 100% for other varieties. The overall accuracy was 86.67%.

In conclusion, based on the planting pattern and the calendar, the reproductive phase of rice plants occurred in the months of (i) late Januari - mid-February, (ii) late May - mid-June, and (iii) late September - mid-October. The linear spectral unmixing algorithm processing using Landsat 8 image data yielded a fraction image for Inpari 32 with a value range of 0.41 to 0.89. Meanwhile, the fraction images of Cibogo and MR exhibit a value range of 0 for each pixel. Similarly, the linear spectral unmixing algorithm processing using Worldview 2 image data produced a fraction image of Inpari 32 with a value range of 0.41 to 1.26. The fraction images of Cibogo and MR also display a value range of 0 for each pixel. Based on the results of the linear spectral unmixing processing on both satellite image datasets, it was evident that the dominant variety used by farmers in Ngawi District during the first planting season of 2023 was the Inpari 32 variety. The accuracy test results using RMSE and Confusion Matrix indicate that Landsat 8 image data achieved the RMSE value of ±1.2% and an overall accuracy of 86.67%. The RMSE of linear spectral unmixing was influenced by the bandwidth range of each satellite image channel. Landsat 8 satellite possesses a narrower bandwidth range compared to Worldview 2 satellite, contributing to a better RMSE value for Landsat 8 relative to Worldview 2.

ACKNOWLEDGEMENTS

This research was partially funded by the Ministry of Education, Culture, Research, and Technology, Republic of Indonesia (grant numbers 0536/E5/PG.02.00/2023; 112/E5/PG.02.00.PL/2023 and 1997/PKS/ITS/2023). Landsat-8 and MODIS data courtesy of the U.S. Geological Survey. Vector data courtesy of the National Geospatial Information Agency (BIG). Field data collection supported by PT. Aria Agri Indonesia. We would like to thank the anonymous reviewers for their valuable comments and suggestions.

REFERENCES

Abdul-Rahaman A, Issahaku G, Zereyesus YA. 2021. Improved rice variety adoption and farm production efficiency: Accounting for unobservable selection bias and technology gaps among smallholder farmers in Ghana. Technol Soc 64: 101471. DOI: 10.1016/j.techsoc.2020.101471.

Bai L, Lin H, Sun H, Mo D, Yan E. 2012. Spectral unmixing approach in remotely sensed forest cover estimation: A study of subtropical forest in Southeast China. Phys Proc 25: 1055-1062. DOI: 10.1016/j.phpro.2012.03.199.

Bandumula N. 2018. Rice production in Asia: Key to global food security. Proc Natl Acad Sci India Sect B Biol Sci 88 (4): 1323-1328. DOI: 10.1007/s40011-017-0867-7.

Bhandari AK, Kumar A, Singh GK. 2012. Feature extraction using Normalized Difference Vegetation Index (NDVI): A case study of Jabalpur City. Proc Technol 6: 612-621. DOI: 10.1016/j.protcy.2012.10.074.

BPS. 2022. Produksi padi Jawa Timur Selama Tahun 2021 sebesar 9,789 Juta Ton Gabah Kering Giling. BPS Jawa Timur, Surabaya. https://jatim.bps.go.id/pressrelease/2022/03/01/1312/produksi-padi-jawa-timur-selama-tahun-2021-sebesar-9-789-juta-ton-gabah-kering-giling.html [Indonesian]

Chandrasekar K, Sesha SMVR, Roy PS, Dwevedi RS. 2010. Land Surface Water Index (LSWI) response to rainfall and NDVI using the MODIS Vegetation Index product. Intl J Remote Sens 31 (15): 3987-4005. DOI: 10.1080/01431160802575653.

Cipta IM, Jaelani LM, Sanjaya H. 2022. Identification of paddy varieties from Landsat 8 Satellite Image Data using Spectral Unmixing Method in Indramayu Regency, Indonesia. ISPRS Intl J Geoinf 11 (10): 510. DOI: 10.3390/ijgi11100510.

Daldegan GA, Roberts DA, Ribeiro FdeF. 2019. Spectral mixture analysis in Google Earth Engine to model and delineate fire scars over a large extent and a long time-series in a rainforest-savanna transition zone. Remote Sens Environ 232: 111340. DOI: 10.1016/j.rse.2019.111340.

Dineshkumar C, Nitheshnirmal S, Bhardwaj A, Priyadarshini KN. 2019. Phenological monitoring of paddy crop using time series MODIS Data. Proceedings 24 (1): 19. DOI: 10.3390/IECG2019-06205.

Gao X, Huete AR, Ni W, Miura T. 2000. Optical-biophysical relationships of vegetation spectra without background contamination. Remote Sens Environ 74 (3): 609-620. DOI: 10.1016/S0034-4257(00)00150-4.

Ghimire R, Huang W-C, Shrestha RB. 2015. Factors affecting adoption of improved rice varieties among rural farm households in Central Nepal. Rice Sci 22 (1): 35-43. DOI: 10.1016/S1672-6308(14)60278-X.

Huete A, Didan K, Miura T, Rodriguez EP, Gao X, Ferreira LG. 2002. Overview of the radiometric and biophysical performance of the MODIS vegetation indices. Remote Sens Environ 83 (1-2): 195-213. DOI: 10.1016/S0034-4257(02)00096-2.

Hussain S, Fujii T, McGoey S, Yamada M, Ramzan M, Akmal M. 2014. Evaluation of different rice varieties for growth and yield characteristics. J Anim Plant Sci 24 (5): 1504-1510.

Kärdi T. 2007. Remote sensing of urban areas: Linear Spectral Unmixing of Landsat Thematic Mapper images acquired over Tartu (Estonia). Estonian J Ecol 56 (1): 19-32. DOI: 10.3176/eco.2007.1.02.

Keshava N. 2003. A survey of spectral unmixing algorithms. Linc Lab J 14 (1): 55-78.

Keshava N, Mustard JF. 2002. Spectral unmixing. IEEE Signal Process Mag 19 (1): 44-57. DOI: 10.1109/79.974727.

Li CH, Tam PKS. 1998. An iterative algorithm for minimum cross entropy thresholding. Pattern Recognit Lett 19 (8): 771-776. DOI: 10.1016/S0167-8655(98)00057-9.

Liang L. 2019. Phenology. In: Reference Module in Earth Systems and Environmental Sciences. Elsevier. DOI: 10.1016/B978-0-12-409548-9.11739-7.

Maraseni TN, Deo RC, Qu J, Gentle P, Neupane PR. 2018. An international comparison of rice consumption behaviours and greenhouse gas emissions from rice production. J Clean Prod 172: 2288-2300. DOI: 10.1016/j.jclepro.2017.11.182.

Otsu N. 1979. A threshold selection method from gray-level histograms. IEEE Trans Syst Man Cybern 9 (1): 62-66. DOI: 10.1109/TSMC.1979.4310076.

Pal NR, Pal SK. 1993. A review on image segmentation techniques. Pattern Recognit 26 (9): 1277-1294. DOI: 10.1016/0031-3203(93)90135-J.

Potter C, Genovese V, Gross P, Boriah S, Steinbach M, Kumar V. 2007. Revealing land cover change in California with satellite data. EOS 88 (26): 269-274. DOI: 10.1029/2007EO260001.

Sarangi SK, Maji B, Singh S, Sharma DK, Burman D, Mandal S, Singh US, Ismail AM, Haefele SM. 2016. Using improved variety and management enhances rice productivity in stagnant flood-affected tropical coastal zones. Field Crop Res 190: 70-81. DOI: 10.1016/j.fcr.2015.10.024.

Singer RB, McCord TB. 1979. Mars: Large scale mixing of bright and dark surface materials and implications for analysis of spectral reflectance. Proc Lunar Planet Sci Conf 10th 2: 1835-1848.

Singh V, Zhou S, Ganie Z, Valverde B, Avila L, Marchesan E. 2017. Rice production in the Americas. In: Chauhan BS, Jabran K, Mahajan G (eds). Rice Production Worldwide. Springer, Cham. DOI: 10.1007/978-3-319-47516-5_6.

Szabó S, Gácsi Z, Balázs B. 2016. Specific features of NDVI, NDWI and MNDWI as reflected in land cover categories. Landsc Environ 10 (3-4): 194-202. DOI: 10.21120/le/10/3-4/13.

Tompolidi AM, Sykioti O, Koutroumbas K, Parcharidis I. 2020. Spectral unmixing for mapping a hydrothermal field in a volcanic environment applied on ASTER, Landsat-8/OLI, and Sentinel-2 MSI satellite multispectral data: The Nisyros (Greece) case study. Remote Sens 12 (24): 4180. DOI: 10.3390/rs12244180.

USDA. 2015. Grain: World Markets and trade, Foreign Agricultural Service. http://www.minagri.gob.ar/new/0-0/programas/dma/usda/grains/2015/2015-12-15.pdf

Wahyudi A, Kuwornu JKM, Gunawan E, Datta A, Nguyen LT. 2019. Factors influencing the frequency of consumers' purchases of locally-produced rice in Indonesia: A Poisson Regression Analysis. Agriculture 9 (6): 117. DOI: 10.3390/agriculture9060117.

Weng Q, Lu D, Schubring J. 2004. Estimation of land surface temperature-vegetation abundance relationship for urban heat island studies. Remote Sens Environ 89 (4): 467-483. DOI: 10.1016/j.rse.2003.11.005.

Xin F, Xiao X, Dong J, Zhang G, Zhang Y, Wu X, Li X, Zou Z, Ma J, Du G, Doughty RB, Zhao B, Li B. 2020. Large increases of paddy rice area, gross primary production, and grain production in Northeast China during 2000-2017. Sci Total Environ 711: 135183. DOI: 10.1016/j.scitotenv.2019.135183.

Xu X, Tong X, Plaza A, Zhong Y, Xie H, Zhang L. 2017. Using linear spectral unmixing for subpixel mapping of hyperspectral imagery: A quantitative assessment. IEEE J Sel Top Appl Earth Obs Remote Sens 10 (4): 1589-1600. DOI: 10.1109/JSTARS.2016.2624560.

Yu J, Chen D, Lin Y, Ye S. 2017. Comparison of linear and nonlinear spectral unmixing approaches: A case study with multispectral TM imagery. Intl J Remote Sens 38 (3): 773-795. DOI: 10.1080/01431161.2016.1271475.

Zhang X, Friedl MA, Schaaf CB, Strahler AH, Hodges JCF, Gao F, Reed BC, Huete A. 2003. Monitoring vegetation phenology using MODIS. Remote Sens Environ 84 (3): 471-475. DOI: 10.1016/S0034-4257(02)00135-9.

Zhao R, Li Y, Chen J, Ma M, Fan L, Lu W. 2021. Mapping a paddy rice area in a cloudy and rainy region using spatiotemporal data fusion and a phenology-based algorithm. Remote Sens 13 (21): 4400. DOI: 10.3390/rs13214400.